Formation of microdischarges inside a mesoporous catalyst in dielectric barrier discharge plasmas

Formation of microdischarges inside a mesoporous catalyst in dielectric barrier discharge plasmas

Ya Zhang[1,2], Hong-yu Wang[3,4], Yu-ru Zhang[2,5], Annemie Bogaerts[2*]

[1] School of Science, Wuhan University of Technology, Wuhan 430074, China
[2] Research group PLASMANT Department of Chemistry University of Antwerp, B-2610 Wilrijk-Antwerp, Belgium
[3] School of Physics Science and Technology, Anshan Normal University, Anshan, 114007, China
[4] Shanghai Bright-Tech Information Technology Co. Ltd, Shanghai, 201206, China
[5] Key Laboratory of Materials Modification by Laser, Ion, and Electron Beams (Ministry of Education), School of Physics and Optoelectronic Technology, Dalian University of Technology, Dalian 116024, China

E-mail: annemie.bogaerts@uantwerpen.be

Abstract. The formation process of a microdischarge in both μm- and nm-sized catalyst pores is simulated by a two-dimensional particle-in-cell/Monte Carlo collision model. A parallel-plate dielectric barrier discharge configuration in filamentary mode is considered in ambient air. The discharge is powered by a high voltage pulse. Our calculations reveal that a streamer can penetrate into the surface features of a porous catalyst and microdischarges can be formed inside both μm- and nm-sized pores, yielding ionization inside the pore. For the μm-sized pores, the ionization mainly occurs inside the pore, while for the nm-sized pores the ionization is strongest near and inside the pore. Thus, enhanced discharges near and inside the mesoporous catalyst are observed. Indeed, the maximum values of the electric field, ionization rate and electron density occur near and inside the pore. The maximum electric field and electron density inside the pore first increase when the pore size rises from 4 nm to 10 nm, and then they decrease for the 100 nm pore, due to a more pronounced surface discharge for the smaller pores. However, the ionization rate is highest for the 100 nm pore due to the largest effective ionization region.

1. Introduction

Microdischarges (MDs) are plasma sources that operate on a continuous basis at gas pressures up to atmospheric pressure by shrinking the dimensions below 1 mm following the famous pd product (i.e., product of pressure and characteristic gap size)[1, 2]. There has been great interest in an atmospheric pressure dielectric barrier discharge (DBD) due to its many applications in environmental, biological, and other fields, including abatement of atmospheric pollutants from air and exhaust gas cleaning. Generally, three discharge modes can be distinguished in DBD: Townsend mode, uniform glow discharge mode and filamentary mode[3, 4].

A DBD plasma is an ionized gas, consisting of various reactive species (electrons, ions, radicals, ...). This reactive environment is created by applying electric power (e.g., a potential difference between two electrodes), mainly heating the electrons in the plasma, while the gas itself remains near room temperature. The energetic electrons can activate the gas by electron impact ionization, excitation and dissociation, creating reactive species, which can easily form new

molecules. This allows the break-up of inert molecules at mild reaction conditions (atmospheric pressure and room temperature) and thus reduced energy costs compared to classical thermal processes. However, this reactive environment makes it that the reactions in the gas phase are not selective. However, the discharge effect can be enhanced if the plasma is combined with a catalyst (e.g., when coating the dielectrics with a catalytic material), attributed to the synergistic effect in plasma-catalysis. The hybrid plasma-catalyst system is very effective for environmental protection, such as air pollution control and greenhouse gas conversion into value-added chemicals[5, 6, 7, 8, 9]. Plasma-catalysis can be defined as any combination of a plasma with a catalyst, resulting in improved processing of the input gas stream. There are two types of setup for plasma catalysis, i.e., single-stage plasma catalysis (the catalyst is positioned inside the plasma) and two-stage plasma catalysis (the catalyst and the plasma are physically separated). Single-stage plasma catalysis is more suitable for a non-thermal plasma, such as a DBD or a corona discharge. The drawback is, however, a limited volume of the MDs, which can be solved by using a porous catalyst due to its large surface area. For instance, a porous catalyst was used for hydrogen production, where the synergetic effect play a role[10]. A monolithic ceramic catalyst combined with a DBD plasma was investigated for the decomposition of acetone, where the results indicated that the combined effects of plasma and porous catalyst led to an enhancement in the decomposition of acetone[11].

Moreover, applications of catalysts both in the plasma discharge zone and as an additional packed bed in an non-thermal plasma have been studied by Holzer et al.[12, 13, 14]. By studying the oxidation of various organic substances immobilised on non-porous and porous catalysts, the authors provided for the first time clear experimental evidence for the presence of short-lived oxidants in the interior of porous catalysts, for a typical pore size of 10 nm in the mesoporous range[12, 13]. The authors distinguished two mechanisms, i.e., (i) the presence of short-lived species in the pore was caused by diffusion, and (ii) these species were generated within the pores if the electric field there was much stronger than in the gas-phase discharge. Furthermore, they speculated that the diffusion of radicals was more plausible than the direct formation of radicals inside the pores. Thus, it is crucial to understand the underlying physicochemical mechanisms for the existing species in a catalyst pore of typically 10 nm.

Hensel et al. investigated the conditions of stable and uniform discharge generation inside ceramic pores, in an atmospheric pressure dry air plasma, with pore sizes of 0.8, 15, and 90 μm[15]. They demonstrated that for the smallest pores (0.8 μm), the discharge developed on the dielectric surface and no discharge inside the pores was observed, whereas for the larger pores, the surface discharge leaked into the ceramics and MDs inside the material were observed above a threshold voltage (i.e., 8.6 kV). The mechanism governing the MD behavior inside the ceramic pores was related to the so-called back-corona phenomenon, which occurred when charges were accumulated on a porous dielectric layer of high resistivity, present at the electrodes. When the voltage drop across the layer exceeded a critical value, an ultimate breakdown through the layer took place and the discharge could leak into the porous ceramic. Thus, an effective generation of MDs inside porous ceramics was possible in hybrid plasma catalyst reactors, but for a specific pore size and discharge power. This mechanism of a back-corona discharge may not be the same as a streamer-induced MD[16, 17]. Indeed, in the latter case, MDs will be generated inside a catalyst pore when the streamer head propagates into the pore.

The same group also applied alternating current (AC) high voltages to generate MDs inside pores, with pore sizes of 50 and 80 μm[18], and a homogenous discharge was observed in nitrogen. However, with the increase of oxygen and carbon dioxide in the mixture, the discharge homogeneity deteriorated. Subsequently, the same authors reported that the formation of microplasmas inside the micropores of ceramic foams was possible only for voltages higher than a specific value determined by the pore size of the ceramics[19]. By means of an AC high voltage source[19], they demonstrated that the onset voltage was too high to generate

MDs inside small pores (less than 2 μm), and there was no repetitive MD formation for large pores (above several hundreds of micrometers) due to the ultimate breakdown between the mesh electrodes. Moreover, Koo et al.[20] investigated the MD formation inside ceramic foams with pores of a few hundred microns for hydrogen generation, and reported that the stability of the MDs was sensitive to the pore size. Finally, Kim[21] investigated the generation of MDs inside a honeycomb type catalytic monolith for NO_x removal, and he found that frequent sparking occurred and resulted into ultimate insulation failure of the catalyst.

All of the above studies were carried out experimentally. Thus the underlying mechanisms for the formation and properties of MDs in a mesoporous catalyst are still poorly understood. Recently, within our group PLASMANT, a two-dimensional (2D) fluid model for a DBD plasma operating in glow discharge mode in helium, was developed, to study the formation of MDs in the interparticle macro (μm) pores in structured catalysts, sustained for various applied (AC) voltages (2 kV -100 kV) and pore sizes (10 μm - 400 μm)[22]. However, the formation of MDs in a mesoporous (nm) catalyst, has not been examined so far. Indeed, the catalyst pore is typically nm-sized[12, 13]. Here we only consider the case of a negative polarity. In fact, for discharges at atmospheric pressure, positive streamers are easier to form than negative streamers, as the electrons can propagate to the anode, scattered by the neutrals and this leads to ionization. However, in our simulations, the gap spacing is so small that the distance is not enough to form positive streamers. Meanwhile, the seed electrons are easier to be generated near the cathode and can be supplemented by the electrons generated by the photo-ionization processes.

In this paper, we investigate, for the first time, the formation and characteristics of MDs in a nm-sized catalyst pore for a filamentary DBD mode, by means of a two-dimensional (2D) particle-in-cell/Monte Carlo collision (PIC/MCC) model. A DBD applied for plasma catalysis applications is usually sustained in a reactive gas mixture, like air, and thus it typically operates in filamentary mode. This means that the DBD is not uniform and consists of numerous MDs, which occur in a number of individual tiny breakdown channels distributed in the discharge gap[23]. The filaments in a DBD are a form of streamer, which propagates due to the space charge separation in the streamer head. Note that in this paper we only consider the effect of pore size, and a dielectric material with a fixed dielectric constant, and we do not consider other material properties in the model, that might play a role in plasma catalysis.

We first investigate the discharge behavior in case of a 10 μm catalyst pore, which is relevant for structured catalysts, in order to be able to simultaneously describe the streamer propagation inside the entire DBD plasma and in the catalyst pore, which is not possible for nm-sized pores because of mesh size problems (see below). The results of this study for the 10 μm catalyst pore will form the starting point for the later description of the streamers inside nm-sized pores. Furthermore, this condition allows us to compare with the earlier fluid modeling results from our group for a helium DBD in glow mode. The outline of the paper is as follows. In section 2, our general model is explained. In section 3.1, the detailed model is presented for the formation and propagation of a streamer inside a DBD with a catalyst pore of 10μm, with the results illustrated in section 3.2, i.e., the calculated electron density, electron impact ionization rate and photo-ionization rate during the streamer propagation process in the entire discharge region. In section 4.1, our model is presented for the generation of MDs in nm-sized catalyst pores, while the corresponding results are shown in section 4.2, i.e., the fundamental mechanisms for the formation of MDs, as well as the MD properties, inside nm-sized catalyst pores, for various pore sizes (in the range of 4-100 nm). Finally, our concluding remarks are presented in section 5.

2. Model and solution method

PIC simulations take advantage of the individual behaviour of charged particles in a plasma, and they can be used to model the kinetics of various species by simulating a reduced number of particles[24], compared to a fluid method. In this work, we adopted the widely used commercial

software VSim, version 7.2 [25], in which we use 2D explicit and electrostatic model.

The equations of motion for electrons and ions are

$$\begin{aligned} \frac{d\mathbf{r}_\alpha}{dt} &= \mathbf{v}_\alpha \\ \frac{d\mathbf{v}_\alpha}{dt} &= \frac{Z_\alpha e}{m_\alpha}\mathbf{E} \end{aligned}$$

where α represents the electrons (e) and ions (N_2^+, O_2^+ and O_2^-), and $\mathbf{r}_\alpha$, $\mathbf{v}_\alpha$, Z_α and m_α are the position, velocity, charge, and mass of electrons, N_2^+, O_2^+ and O_2^- ions, respectively.

We use absorption boundary conditions for the particles, i.e., all particles will be removed if they move out of the simulation region or hit the surface of the metal or dielectrics. In addition, when the particles are absorbed by the dielectrics, they have the possibility to emit a secondary electron and they will deposit their charge on the dielectric. This is accounted for by $Q_D = Q_D + Q_p - Q_{see}$, where Q_D is the accumulated charge with increasing time provided that initially $Q_D = 0$, Q_p is the total charge of the electron and ion charges when they striking the dielectric surface, and Q_{see} is the secondary electron charge, respectively. Indeed, we consider perfect dielectrics with no conductivity and no charge leaking. Note that here we assume no initial deposited charge on the dielectrics. In DBD like discharges, charges can accumulate on the surface, which affects the next discharge when the polarity is reversed. Hence, in this work we only consider the first discharge. Indeed, the decay time of surface charges is in the order of seconds[26], thus the assumptions made in the model are valid for the first discharge (maximum simulation time 25 ps) considered here.

The electric field $\mathbf{E}$ is determined by solving the Poisson equation, including the effect of the dielectrics (see below) and the charge deposition, $\nabla \cdot \mathbf{D} = \rho_{tot}$, based on the total charge density ρ_{tot}, which includes the charge densities of electrons and the three types of ions. These charge densities are obtained from direct summation and extrapolation of the species positions, which are calculated above with the equations of motion. Here $\mathbf{D} = \epsilon\mathbf{E}$ is the electric displacement field, $\epsilon = \epsilon_r\epsilon_0$ is the permittivity of the medium, and ϵ_0 is the vacuum permittivity. For simulating the electric potential in the Poisson equation, Dirichlet boundary conditions are used in the y direction, and Neumann boundary conditions are employed in the x direction. The Poisson equation is solved in both the discharge gap and the dielectrics, whereas the equations of motion of particles are solved only in the discharge gap.

The discharge gap is filled with the gas mixture $N_2/O_2 = 80/20$ at atmospheric pressure and 300 K, since this kind of gas mixture typically gives rise to a filamentary discharge in a DBD[16]. The species tracked by the PIC method are, electrons (including electrons in the discharge volume and deposited electrons), and ions (including N_2^+, O_2^+ and O_2^- ions). These three types of ions are the most important, since their threshold energies are much lower, leading to a higher density compared to other ions. The density of the background neutral gas (N_2, O_2) at a temperature of 300 K can be assumed to be static.

The secondary electron emission (SEE) coefficient is assumed to be 0.1 for N_2^+ and O_2^+ ions on the dielectric surface. To examine the impact of this assumption, we performed calculations for different values of the SEE coefficient (i.e., 0.1, 0.2, 1), and we found that this choice did not affect the discharge behavior. The reason is that in streamers, the electrons gain energy more effectively near the streamer head, as there is strong charge separation and a stronger electric field. DBD discharges are characterized by two modes. The first one is the glow-like discharge, as described by Lazarou et al.[27]. The plasma has a lifetime over 100μs, it is uniform and has a steady cathode sheath. The secondary electrons emitted from the surface, are accelerated in the sheath and produce significant ionization in the sheath and bulk plasma. Therefore, they have a significant impact on the discharge. The second mode is the streamer-like discharge that we considered here, which has a lifetime of about 1ns, so the time duration is very short, there is

no sheath, the electrons mainly are accelerated by the strong electric field in the streamer head, and produce most of the ionization nearby the streamer head. The streamer is directed from the cathode to the anode. Here most secondary electrons are emitted from the lower dielectric surface bounded by the anode, and they are trapped there. Note that there is no sheath. Thus the emitted secondary electrons will not reach the streamer head, and they will not feel this strong electric field at the streamer head. So according to our results, the secondary electrons play a minor role. Indeed, we have found that the results are nearly the same with and without SEE in our simulations, so the effect of secondary electron emission can be neglected.

The electron impact reactions are incorporated in the simulation by applying a MCC scheme that statistically determines the particle scattered velocities after collisions. We consider 23 reactions, including elastic, excitation, ionization and attachment collisions of electrons with N_2 and O_2 gas molecules, as listed in Table 1, where the threshold energies are adopted from the LXCat database and literature[28, 29, 30, 31]. The collision data for nitrogen N_2 and oxygen O_2 are downloaded from the LXCat database[32]. The collisions for nitrogen and oxygen that we have adopted in this work are the ones listed in the Vsim 7.2 software package. They are adopted from the LXcat database, but the software has made some modifications for the collision processes and cross sections, by combining some levels. Thus, only the reactions listed in Table 1 are considered in this work.

3. Complete streamer in a DBD with a catalyst pore of 10 μm

3.1. Model

The geometry used in the model is shown in Fig. 1. The simulation region is 300 μm $\times$300 μm. The planar parallel electrodes are covered by SiO_2 ($\epsilon_r = 4$) dielectrics. A catalyst pore in the bottom dielectric plate is considered. The diameter of the pore is 10 μm and the depth is 80 μm (see Fig. 1). Note that in the rest of this paper, we used the term "pore size" when referring to the pore diameter. The discharge gap is 100 μm, and the plasma region is bounded by two dielectric plates with a thickness of 100 μm. A pulsed voltage of -10 kV with a rise time of 1 fs is applied to the top electrode, and the bottom electrode is grounded. The voltage is held constant after the rise time. The number of uniform mesh points is 500×500 in the entire computational region (i.e., 300 μm $\times$300 μm). The total simulation time is 25 ps which takes about 72 hours on a duel-core computer.

The streamer is initiated by artificially emitting seed electrons with a current density of 10^5 A m^{-2} from the middle of the top dielectric surface ($x \in [149, 151]$ μm, $y \in [199, 200]$ μm). This kind of seed electrons can occur by cosmic radiation. Subsequently the streamer develops itself by electron impact ionization and photo-ionization. The number of electrons and ions rapidly increases mainly by the electron impact ionization during the streamer propagation. Thus a particle merging algorithm is used when the number of super-particles exceeds 10 in each mesh, where one super-particle can contain up to 10^{11} real particles. In this case, 4 super-particles are combined into 2 super-particles under the conservation of both momentum and energy. The simulation time-step dt is chosen to satisfy the Courant limit

$$cdt < \frac{1}{\sqrt{(\frac{1}{dx})^2 + (\frac{1}{dy})^2}} \tag{1}$$

, where c is the light velocity, and dx and dy are the spatial steps in x and y direction, respectively. Radiation transport and photo-ionization are described as follows.

Photo-ionization is an important process in simulating the streamers propagation. However, photo-ionization is not supported directly by VSim, therefore we have coupled some Python code to include this. Our model for photo-ionization is briefly discussed as follows:

In air ($N_2/O_2 = 80/20$), photo-ionization likely occurs from excited states of nitrogen. Photo-ionization of oxygen is considered by absorption of photons emitted by $N_2(b^1\Pi)$ and $N_2(b^1\Sigma)$

with a wavelength of $98-102$ nm and a cross section of 10^{-22} m^{-2} according to the literature[33]. The reaction mechanism is listed in Table 1. Note here we have made some simplification in the processes in order to make the results more clear and speed up the calculations, by omitting less important processes. We have tested whether including these processes will not affect the results significantly. Indeed, the cross sections datasets for one species can be very different from data to data. But still, we have got reasonable results with omitting less important processes. Here, the excitations that are related to photo-ionization and ionisation are dominant processes and all of which are correctly considered.

Three main steps are taken to include photo-ionization in this VSim simulation.

First, the radiation source $\lambda\rho_I$ is obtained from the excitation rate S of $N_2(b^1\Pi)$ and $N_2(b^1\Sigma)$. Here $\lambda = 2 \times 10^5$ s^{-1} is the rate coefficient of the radiation reaction shown in Table 1[34, 35]. ρ_I is given from the equation

$$\frac{d\rho_I}{dt} = S - \lambda\rho_I. \tag{2}$$

Second, the radiation transport equation, simplified as a diffusion equation

$$\frac{\partial I}{\partial t} = D_I\nabla^2 I + \lambda\rho_I. \tag{3}$$

is inserted into the equation solver code, where I is the radiation density field and D_I is the diffusion coefficient taken as 300 μm $\times$300 μm/dt.

Third, the photo-ionization rate is initially given from the radiation density field I at initial time, the density of the oxygen and the cross section for the photo-ionization. Next, the space-time changed photo-ionization will be simulated self-consistently, based on the space-time dependent radiation density field I.

3.2. Results and discussion

In order to provide the property of a streamer when a catalyst pore is included in a DBD reactor, the time evolution of the electron density is shown in Fig. 2. The formation and propagation of the streamer is clearly seen. The pore size is 10 μm as shown in Fig. 1. The electrons are rapidly multiplied from a few seed electrons by electron impact ionization and photo-ionization, and they form an anode-directed streamer. The streamer head arrives at the bottom of the pore at 15 ps, and the maximum electron density inside the discharge gap increases rapidly from 8×10^{19} to 2×10^{23} m^{-3}. Thus, one can roughly estimate the average propagation speed of the streamer to be about 10^7 m/s, which is a factor 10 higher than that of a streamer in a DBD reactor with the same applied voltage but a much larger discharge gap[16]. This is due to the higher electric field ($\sim 10^8$ V/m) for the smaller discharge gap of 100 μm, compared to the lower electric field $\sim 10^7$ V/m for the larger discharge gap of 1 mm in literature[16] under the same applied voltage. When the streamer penetrates into the pore, the electron density inside the pore exhibits a significant increase within about 10 ps, as shown in Fig. 2(d-f). This indicates that a MD is generated inside the pore by itself as the streamer head penetrates into the pore, rather than due to diffusion or migration of plasma species into the pore. This will be further verified from figure 3. This phenomenon was also investigated experimentally by Hensel et al[15, 18, 19] for a corona discharge, as the surface discharge leaked into the catalyst pore.

It should be mentioned that in previous work from our group, Zhang et al.[22] have reported that no significant increase of the electron density and ionization occurred inside a 10 μm pore. This difference is attributed to the different conditions. Indeed, the study of Zhang et al.[22] was applied to a helium DBD operating in glow mode, which is characterized by a much lower electron density (10^{17} m^{-3}), and thus a much larger Debye length $\lambda_{De} = \sqrt{\epsilon_r\epsilon_0 T_e/ne^2}$ of 40 μm. In this formula, T_e is the electron temperature in eV, n is the electron density in m^{-3}, and e is the electron charge in C. This Debye length is clearly larger than the pore size, indicating that

a glow-like plasma, consisting of a bulk region and sheaths near the walls, cannot be developed in the pore. On the other hand, in the present study, the DBD operates in filamentary mode, where the maximum electron density is 10^{23} m^{-3} and the Debye length is 40 nm. As this Debye length is smaller than the pore size, this explains why a MD, that is induced by a streamer in the filamentary mode, can be formed in a 10 μm pore.

In order to understand the reasons of the electron density enhancement inside the catalyst pore, we plot the electron impact ionization rate (a) and photo-ionization rate (b) in Fig. 3. Note that there is no background photo-ionization. Photo-ionization is originally due to excited states of nitrogen. In the discharge region, photo-ionization generates electrons and ions, in addition to those generated by electron impact ionization, but the electron impact ionization is dominant for the negative streamers[36].

The streamer reaches the bottom of the pore at 15 ps. Within about 10 ps, when the streamer has entirely penetrated into the pore, the electron impact ionization rate inside the pore increases rapidly, which agrees well with the evolution of the electron density (see Fig. 2). Indeed, the electron impact ionization rate reaches its maximum inside the pore at 25 ps, and the value is nearly one order of magnitude higher than in the bulk. This gives rise to the high electron density inside the pore. Furthermore, the electron impact ionization rate as well as the photo-ionization rate profiles confirm the fact that the MD is really generated inside the pore. Zhang et al.[22] have also calculated a similar electron impact ionization rate profile with their fluid model, showing the maximum values in the pore, but for much larger pores. Note that there is almost no photo-ionization at 5 ps. At 10-25 ps, the maximum value of the photo-ionization rate is two orders of magnitude smaller than the electron impact ionization rate. Indeed, Kushner et al. also reported that the rate of photo-ionization was two orders of magnitude smaller than that of electron-impact ionization, for a large discharge gap ($\sim$1 mm)[33, 16]. However, the presence of photo-ionization extends the ionization region (see Fig.3) as well as the region of the electron distribution (see Fig. 2 above) to greater distances. At 15 ps, the electron impact ionization rate is higher than 10^{17} $m^{-3}s^{-1}$ in the central streamer region, while the photo-ionization rate is lower than 4×10^{15} $m^{-3}s^{-1}$ outside of this region. What is important is that photo-ionization has not changed the character of the streamer propagating into the pore.

4. Plasma formation in a mesoporous catalyst

4.1. Model

In this model, we investigate the behavior of electrons and ions inside nm-sized catalyst pores, by means of the same PIC/MCC model, but there are some significant differences, as will be explained below. We focus especially on nm-sized pores, which are most common for catalyst materials[12, 13]. The discharge gas (atmospheric pressure dry air: $N_2/O_2 = 80/20$) and chemical reactions, as well as the PIC/MCC method, are the same as in the general model described in section 2, and are therefore not repeated again. Due to the huge differences in the dimensions of the discharge gap and the nm-sized pore, and the fact that the VSim simulation package used to run the PIC/MCC model does not allow the use of a non-uniform mesh size[25], it is impossible to simulate the whole region and the pore simultaneously. Indeed, Lapenta et al. also predicted that the PIC method is not really suitable for using a non-uniform grid[37]. Hence, we only simulate a small region near the catalyst pore, applying as boundary condition the results of the streamer that has already reached this region, with initial number density of 10^{23} m^{-3} and velocity of 10^7 m/s, as obtained from our self-consistent PIC/MCC simulation of a streamer in a DBD reactor with a gap of 100 μm and a pore of 10 μm(see previous section). The propagation velocity obtained from our model is quite high. The reason is that a high pulsed voltage of 10 kV is applied over a small discharge gap of 100 μm, yielding a strong electric field. This velocity is one order of magnitude higher than obtained by Babaeva and Kushner[16], but the authors considered the same voltage but a much larger gap of 1 mm. Hence, the electric field

in our case in one order of magnitude higher, which can explain why the propagation velocity is also one order of magnitude higher. Therefore, we believe that this result is reasonable, although we did not find any experimental data in literature to verify this.

The geometry used in the model is shown in Fig. 4. As we do not simulate the entire discharge region as in previous section, we assume a pulsed voltage of -100 V with a rise time of 1 fs, applied at a (dummy) powered electrode, located at 2 μm from the grounded electrode, or 1 μm from the top of the dielectric layer (see Fig. 4). This assumption is based on the potential drop near the pore obtained with the model of previous section. A catalyst pore is present in a 1 μm thick SiO_2 dielectric plate placed above the grounded electrode located at $y = 0$. The discharge gap between the dielectric layer and the dummy powered electrode is thus fixed at 1 μm. In the x direction we also consider only a small section of the discharge, equal to a length of 0.3 μm, since the streamer properties near and inside the pore are most important. Note that, in order to clearly show the pore in space dimension, only the central part including the pore is indicated in Fig. 4(a-b), although the simulation region in practice extends from 0 to 0.3 μm in the x direction, like in Fig. 4(c).

First, the propagation of the streamer is investigated for a fixed pore size (10 nm). Subsequently, the MD properties inside the catalyst pore will be investigated for various pore sizes (4, 10, 50 and 100 nm), by examining the spatial profiles of the electric field, electron density, electron impact ionization rate and electric potential inside the pores, as well as the negative surface charge density, and the electron trajectory inside the pores. We assumed that the pores are always vertical with a depth 8 times larger than the diameter. As written above, the pore size refers to the pore diameter. Note that photo-ionization is not considered for the nm-sized pores, since the wavelength of the photons is in the range $98-102$ nm, which is larger or comparable to the nm pores[33]. Thus the photons are absorbed without producing ionization. Furthermore, the simulation time is so short ($\leq$ 1.2 ps) that photo-ionization can be neglected [see Fig. 3(b) in previous section: the photo-ionization is small even at 5 ps].

4.2. Results and discussion

4.2.1. Plasma formation in a mesoporous catalyst Fig. 5 shows the time evolution of the electron density, which indicates the penetration of a streamer into a mesoporous catalyst and the plasma formation process inside the pore. The pore size is 10 nm and the pore depth is 80 nm. Note the different dimensions of Fig. 5(a-c) in the y-direction, which is needed to illustrate the streamer propagation. At 0.2 and 0.28 ps, the plasma is very weak near the pore, because the streamer is still far away from the pore, as shown in Figs. 5(a-b). At 0.32 ps, there is also no plasma in the pore, because the streamer has still not yet entered into the pore, as shown in Fig. 5(c). The streamer enters the pore at 0.36 ps, and the electron density reaches its maximum values in the pore, as shown in Fig. 5(d). This indicates the importance of pores for plasma-catalysis applications, as the plasma can be clearly enhanced inside the pores, leading to a larger surface area of the catalyst material exposed to the plasma species. The streamer reaches the bottom of the pore at 0.4 ps, and the electron density inside the pore is further enhanced. Moreover, a high electron density also appears near the dielectric outside the pore (see Fig. 5(c)). As is clear from Fig. 5(d), the electron density profile inside the pore remains constant up to at least 1.2 ps, but the maximum density is now only found above and inside the pore. The time evolution of the electron density in the case of this 10 nm pore is thus quite similar to that shown in Fig. 2 for the 10 μm pore, of course keeping in mind the different space and time scales. Note that the total ionization rate is not very high (i.e., ionization degree $\leq 10\%$) in this VSim simulation. Therefore, the upper plasma density limit of our simulation is about 2.5×10^{24} m^{-3}. At 0.4 and 1.2 ps, the red color represents a density value of 2.1×10^{24} m^{-3}, which is more or less the maximum electron density reached. Only in some very small regions the electron density can reach a value of 3×10^{24} m^{-3}, as indicated by the dark red color

in Fig. 5(e-f). The electron density is very high, and at first sight, this seems unexpectedly high. Indeed, in glow-like DBD discharges, the plasma is quite uniform and the plasma density would be much lower. However, in our case the discharge is driven by a pulsed voltage with amplitude of 10kV in a narrow gap. Hence, it is streamer-like or even arc-like, not glow-like, and in these kinds of discharges, the plasma density can be very high. The density is indeed comparable with experimental data obtained at comparable conditions[38].

Note that the Debye length is around 10 nm under these conditions, since the maximum electron density is above 10^{24} m^{-3}, thus the pore size of 10 nm is comparable to the Debye length, which indeed suggests that plasma species can be generated inside a mesoporous (2-50 nm) catalyst, like HY zeolites[39]. Bhoj and Kushner[40] also reported that plasma species for a corona discharge in humid air were able to penetrate into a rough polymer surface with a limited extent for a pore size of about 1 μm. This pore size was comparable to the Debye length in their work. Besides, Zhang et al.[22] predicted that plasma species can be formed inside the interparticle macro (μm) pores in structured catalysts, with pore sizes comparable to or larger than the Debye length, which was 40 μm in their work.

In order to clearly understand the time evolution of the MD formation process, Fig. 6 shows the electron impact ionization rate at the same times as in Fig. 5. Note that the profiles are not very smooth (in this and some following figures). We cannot improve the results by statistics, because our simulation is an evolutionary simulation, and averaging cannot be used, and the history of the simulation will also be part of the final result.

However, we believe that the physics is captured well by our model, in spite of the approximations. It is clear from Fig. 6 that the maximum ionization rate is enhanced with increasing time, especially after the streamer has reached the bottom of the pore. When the streamer propagates into the pore at 0.36 ps and reaches the bottom at 0.4 ps, the ionization rate takes its highest values in the pore. However, after the streamer has filled the entire pore, i.e., at 1.2 ps, the maximum ionization rate occurs both inside the pore and above the pore, as seen from Fig. 6(f). This is because the electric field is the strongest at both the top and bottom of the pore, as will be presented in Fig. 7(b), yielding a higher ionization efficiency.

Note that when the streamer head penetrates into the pore, the gas in the pore will directly breakdown by the high electric field at the streamer head, and the pores are filled by the charged particles in the streamer. This kind of plasma formation is not affected by the ionization mean free path, in contrast to homogenous ionization caused by electron impact ionization collisions. This can explain why plasma formation can occur in pores of 10 nm, even when the mean free path in air is about 60 nm at atmospheric pressure.

4.2.2. Effect of pore size on the MD behavior inside the pores It was reported experimentally[15] and computationally[22] that the pore sizes can influence the formation of the MD inside a μm-sized catalyst pore. However, the effect of the pore size in the nm range on the MD behavior has not been investigated yet. Therefore, we simulate various plasma characteristics, i.e., the electric field, electron density, electron impact ionization rate, plasma potential, the negative surface charge density on the dielectric surface, and electron trajectory for various pore sizes (between, 4 nm and 100 nm) at 1.2 ps, when the streamer has completely filled up the pore. Since the result for the 50 nm pore is similar to that for the 100 nm pore, we show the results only for the 4, 10 and 100 nm pores.

It has been proposed in literature[12] that a higher electric field inside the pore than that in the bulk discharge gap, may induce the MD generation inside a catalyst pore. Fig. 7 clearly shows that the presence of a catalyst pore, inducing a sharp boundary, strongly enhances the displacement electric field inside the dielectric material near the bottom of the pore. As a result, the electric field inside the pore will also be stronger in this region. Indeed, the local electric field at the bottom of the pore is strong due to the significant charge accumulation at this position

(see Fig. 11 below). Moreover, the electric field at and above the surface of the dielectric is also quite strong for the 4 and 10 nm pores, due to the higher negative surface charge density than for the 100 nm pore (see Fig. 11 below). Indeed, for the 100 nm pore, the discharge is dominated by a volume discharge (as will be explained below), hence the negative surface charge accumulation mainly occurs on the pore boundaries rather than at the dielectric boundary outside the pore (see Fig. 11 below). On the other hand, for the 4 and 10 nm pores, both the volume and surface discharges are important due to the relatively larger surface area than in case of the 100 nm pore.

Note that we plot the total electric field in Fig. 7, which is calculated by ($\sqrt{E_x^2 + E_y^2}$). Here E_x and E_y, are the x component and y component of the electric field, respectively. As the electron mass is much smaller than the ion mass, the electrons run faster and they enter the pore first, leaving the ions behind them. Thus, the electric field E_y directs downwards at the top of the pore, and the positive ions are accelerated inside the pore, while the electrons are pushed out of the pore. This also explains the behavior seen in Figs. 5(b-c-d), where the maximum of the electron density first reaches the bottom of the pore at 0.4 ps, but it disappears at later times, and the peak value occurs above the pore at 1.2 ps.

Fig. 8 shows the electron density distributions for various pore sizes. The maximum electron densities are found inside and straight above the pores for the 4 and 10 nm pores, due to the enhanced electric field at the bottom of the pore and above the dielectric outside of the pore. For the 4 nm pore, the electron density near the bottom of the pore is much lower than at the top of the pore, because the electric field at the top of the pore pushes the electrons upwards, but at the same time, the enhanced electric field at the dielectric boundary outside the pore pushes the electrons back into the 4 nm and 10 nm pores, which gives rise to a maximum electron density at the top of the pore. For the 100 nm pore, the maximum electron density only appears inside the pore, because the electric field is only enhanced at the bottom of the pore.

From Fig. 9, it is clear that the ionization rate in case of the 4 nm pore appears above the pore, while it exists both inside and above the pore, for the 10 nm pore. For the 100 nm pore, on the other hand, the maximum ionization rate is clearly at the top inside the pore. The reason is that the local electric field due to the space charge separation in the pore pushes the electrons out of the pore, inducing many ionization collisions near the top of the pore. This can also be understood as the generation of a positive streamer (cathode-directed) when the negative streamer has filled up the pore, as will be clearly seen from the electron trajectory (see Fig. 12 below). Moreover, the maximum ionization rate increases drastically with pore size, which is different from the electron density evolution (see Fig. 8). This is because, on the one hand, when the pore size increases from 10 nm to 100 nm, the maximum local electric field decreases, leading to a lower electron density, but on the other hand, the effective ionization region increases with pore size, so there are more electrons available to generate ionization, resulting in a higher ionization rate.

Fig. 10 illustrates the potential distributions in the pore and in the dielectric plate around the pore, for the same pore sizes as in previous figures. Note that the asymmetry in the equipotential lines (mainly visible in Fig. 10(a)) is because a filamentary discharge is always asymmetric[41]. Indeed, the asymmetry comes from the inherent statistical properties of the streamers. Streamers are fully chaotic and thus, they may be different even if all the conditions are identical. This is essentially different from low pressure capacitively coupled plasma. The potential increases (i.e., it becomes less negative) from the top of the pore to the bottom, which leads to the non-zero electric field in the pores. The potential difference between top and bottom of the pore is quite limited for the 4 and 10 nm pores (i.e., only a few V), while it is somewhat larger (almost 40 V) for the 100 nm pore. However, the latter pore is 10 times deeper than the 10 nm pore, so the electric field created is quite similar or even somewhat lower, as was seen from Fig. 7 above.

For the 4 and 10 nm pores, the potential is rather constant in the upper part of the pore,

i.e., around -53 V for 4 nm while -56 V for 10 nm, but it rises slightly at the bottom of the pore, over a distance of 10-20 nm, leading to the strong electric field there (see Figs. 7(a) and 7(b)), whereas the potential increases almost linearly from the top of the 100 nm pore to the bottom. Moreover, for the 4 and 10 nm pores, the potential rise in the dielectric layer is somewhat faster than inside the pore. A similar potential distribution in a dielectric layer has also been observed by Kushner et al. for a filamentary DBD mode[16] in humid air. The voltage over the thickness of the dielectric layer under the pore can be deduced from Fig. 10. It is -51.8, -54.48 and -18 for the 4, 10 and 100 nm pore, respectively, as the bottom of the dielectric is grounded. Thus, the equipotential lines are somewhat more curved for the 4 nm pore, and especially for the 10 nm pore, while they are mostly flat for the 100 nm pore. These curved equipotential lines are attributed to the negative charge accumulation on the dielectric surface, which is the strongest in the 10 nm pore and stronger in the 4 nm pore than in the 100 nm pore, as will be shown in Fig. 11 below. This will strongly enhance the electric displacement field inside the dielectric material and near the interface between the dielectric and the pore. Since the dielectric surface area becomes relatively smaller for the larger pores, the effect of the charge accumulation due to the deposited electrons on the dielectric layer becomes of lower importance for the 100 nm pore, giving rise to more uniform equipotential lines in both the dielectrics and the gas.

Fig. 11 shows negative surface charge density for the same pore sizes as in Figs. 7-10, which is determined by counting the absorbed electrons on the dielectric surface. The maximum negative surface charge density appears inside the pore for all three cases. The maximum negative surface charge density becomes higher when the pore size increases from 4 nm to 10 nm, but the value becomes one order of magnitude lower in the 100 nm pore, which can explain the potential distribution and the electric field distribution, as outlined above. In our group, Zhang et al. also obtained the largest negative charge density at the pore bottom [42].

In order to further understand the mechanisms behind the MD generation in a mesoporous catalyst, the trajectories inside the pore for three sample electrons, and for the three different pore sizes, are shown in Fig. 12. Note that these sample electrons are chosen as they can run out of the pore, because once the electrons are deposited on the dielectrics at the boundary of the pore they will not participate in the discharge anymore. However, the deposited electrons can contribute to the negative surface charge density as well as to the local electric field near the dielectric surface. The trajectories for the 4 and 10 nm pores show that the electrons are pushed out of the pore immediately when they enter the pore, by the electric field at the top of the pore. On the other hand, two sample electrons can stay a bit longer in the 100 nm pore, due to the lower electric field and the larger pore size.

Finally, we plot in Fig. 13 the maximum electric field, electron density and ionization rate as a function of pore size. The maximum electric field and electron density first increase when the pore size rises from 4 nm to 10 nm, and then they decrease at 50 nm, and finally a slight increase is observed again from 50 to 100 nm. The same behavior is seen for the ionization rate, but the rise from 50 to 100 nm is much more pronounced, and is attributed to the larger effective ionization region inside the pore, so there are more electrons available to cause ionization, yielding a higher ionization rate, as explained above.

The initial rise in maximum electric field, electron density and ionization rate when increasing the pore size from 4 to 10 nm, followed by the drop in these values when further increasing the pore size to 50 nm, can be explained as follows. As is well known, MDs are generated by a locally inhomogeneous electric field for a filamentary DBD mode and they move along the dielectric surface, namely as a surface discharge[15, 43], which is enhanced with increasing relative surface area. On the other hand, volume discharges increase with gap spacing in a DBD[43]. When the pore size increases from 4 nm to 10 nm, both the surface and volume discharges become stronger, leading to a higher electron density. On the other hand, when the pore size rises from 10 to 50 nm, the surface discharge becomes weaker and the volume discharge is not yet strong

enough, resulting in a lower electron density. As the pore size rises further to 100 nm, although the surface discharge is weak, the volume discharge becomes stronger, giving rise to a slight increase in the electron density.

In general, in a DBD reactor driven by a pulsed voltage, the maximum electric field and electron density are dominated by the surface discharge, and they depend strongly on the local properties, while the ionization rate is dominated by the volume discharge, and this also explains why the maximum ionization rate increases more significantly than the maximum electric field and electron density, when increasing the pore size from 50 to 100 nm. As mentioned in the literature[43, 16, 17] the deposited electrons on the dielectric surfaces could charge the surfaces and trap the electric potential lines in the dielectric. As a result, the voltage drop as well as the electric field in the gap will be reduced, and meanwhile the local electric field inside and near the dielectrics is enhanced due to the locally deposited charges on the dielectric surface (see Fig. 11). Indeed, the applied potential difference between both electrodes causes the dielectric material to polarize. Thus, at the boundary between the dielectric and the gas phase there will be local charges of opposite sign close together, which leads to the locally enhanced electric field near the boundary, which could be clearly seen from Fig. 7.

Last but not least, we briefly discuss the validation of our model. We have applied a 2D electrostatic PIC/MCC model. This model should be valid at the conditions under study, for the following reasons: (1) The plasma density in our case is very high, but it only exists in some small regions, and even with this highest density, the ionization degree is at maximum about 10%. The streamer lifetime is very small ($<$ 1ns), and the energy deposition is not very high. Therefore, the gas heating and depletion can be neglected. If the streamer duration would be longer, the gas heating should be considered. Furthermore, if the ionization degree would be higher than 20%, the MCC model would need to be revised, like in our recent work[44]. However, this is not the case here. (2) Moreover, because the streamer lifetime is short, numerical heating is not important and will not affect our results. (3) The electric field is very strong and the plasma current is quite low, and therefore the electrostatic model is valid and we do not need to use an electromagnetic model.

5. Conclusion

In conclusion, we have presented a 2D PIC/MCC model, obtained with the VSim simulation code, to study the formation and properties of MDs in catalyst pores with various sizes (both the μm and nm range). We investigated the MD formation as the streamer penetrates into the pores. The calculations are performed for an atmospheric pressure dry air DBD in a filamentary mode sustained by a high voltage pulse. A streamer is initiated from seed electrons from the middle of the top dielectric surface.

First, the MD formation is investigated in detail for a fixed pore size (10 μm) and a pulsed voltage of -10 kV with a rise time of 1 fs. The electron density as well as the electron impact ionization rate increase rapidly when the streamer penetrates into the pore, and MDs inside the catalyst pore are observed. Indeed, the maximum values of the electron impact ionization rate and electron density take place inside the pore.

Second, we investigated the MD formation in nm-sized catalyst pores. Our model predicts that the streamer can penetrate into a mesoporous catalyst and MDs can be formed inside the pore, for all pore sizes simulated, i.e., between 4 nm and 100 nm. Our calculation results indicate that the ionization mainly takes place near or inside the pore, due to the strong local electric field at the bottom of the pore caused by the deposited electrons on the dielectric surface, and this leads to a high electron density near and inside the pore. The maximum electric field and electron density first increase when the pore size rises from 4 nm to 10 nm, and then they decrease for the 50 nm pore, followed by again a small rise for the 100 nm pore. This is because the smaller pores have a more pronounced surface discharge along the dielectric surface due to

the relatively larger surface area compared to a larger pore. Indeed, the displacement electric field in the dielectric and at the bottom of the pore is mostly enhanced for the smaller pores. However, the ionization rate is more pronounced in larger pores due to the larger effective ionization region. Indeed, the ionization rate not only depends on the maximum electric field but it is also influenced by the effective volume for ionization.

The active surface area of the porous catalyst as well as the surface reactions will be enhanced if the plasma is combined in a catalyst. The results obtained in this work are of strong interest for plasma catalysis and mesoporous catalysts, because the presence of MDs inside a porous catalyst affect this active surface, and thus the surface reactions, as well as the physical and chemical properties of the catalyst, through both the surface discharge and volume discharge.

It must be realized that the current PIC/MCC simulations, carried out with the VSim code, have limitations, due to constraints in the grid size, which should be very different in the nm-sized pore and the bulk discharge gap. This explains why our simulation results do not look very smooth. Unfortunately, we cannot improve this further with the VSim code. However, in our future work, we will adopt an implicit 2D electromagnetic PIC/MCC code, which implements the so-called multi-level multi-domain (MLMD) method[37], to study both the nm and μm scales. This MLMD method will allow us to use much finer grids near the pore and coarser grids in other regions, independently. Thus, by adopting the MLMD method, we hope to be able to self-consistently solve the physical scales both in μm and nm sized porous catalysts.

6. Acknowledgments

This work was supported by the NSFC (11405067, 11275007, 11375163). Y Zhang gratefully acknowledges the Belgian Federal Science Policy Office for financial support. The authors are very grateful to Wei Jiang for the useful discussions on the photo-ionization model and the particle-in-cell/Monte-Carlo model.

7. References

[1] Kushner M J 2004 *Journal of Applied Physics* **95** 846–859
[2] Bruggeman P and Brandenburg R 2013 *Journal of Physics D: Applied Physics* **46** 464001
[3] Kogelschatz U 2003 *Plasma Phemistry and Plasma Processing* **23** 1–46
[4] Nikandrov D and Tsendin L 2005 *Technical Physics* **50** 1284–1294
[5] Chen H L, Lee H M, Chen S H, Chao Y and Chang M B 2008 *Applied Catalysis B: Environmental* **85** 1–9
[6] Van Durme J, Dewulf J, Leys C and Van Langenhove H 2008 *Applied Catalysis B: Environmental* **78** 324–333
[7] Chen H L, Lee H M, Chen S H, Chang M B, Yu S J and Li S N 2009 *Environmental Science & Technology* **43** 2216–2227
[8] Whitehead J C 2010 *Pure and Applied Chemistry* **82** 1329–1336
[9] Neyts E and Bogaerts A 2014 *Journal of Physics D: Applied Physics* **47** 224010
[10] Hou D, Zhou W, Zhou K, Zhou Y, Zhong J, Yang L, Lu J, Li G and Chen S 2015 *Journal of Materials Chemistry A* **3** 15962–15968
[11] Trinh H Q and Mok Y S 2014 *Chemical Engineering Journal* **251** 199–206
[12] Holzer F, Roland U and Kopinke F D 2002 *Applied Catalysis B: Environmental* **38** 163–181
[13] Roland U, Holzer F and Kopinke F D 2005 *Applied catalysis B: environmental* **58** 217–226
[14] Holzer F, Kopinke F D and Roland U 2002 *Plasma Chemistry and Plasma Processing* **25** 595–611
[15] Hensel K, Katsura S and Mizuno A 2005 *IEEE Transactions on Plasma Science* **33** 574–575
[16] Babaeva N Y and Kushner M J 2014 *Plasma Sources Science and Technology* **23** 065047
[17] Zhang Y, Wang H y, Jiang W and Bogaerts A 2015 *New Journal of Physics* **17** 083056
[18] Hensel K, Martišovitš V, Machala Z, Janda M, Leštinskỳ M, Tardiveau P and Mizuno A 2007 *Plasma Processes and Polymers* **4** 682–693
[19] Hensel K 2009 *The European Physical Journal D* **54** 141–148
[20] Koo I G, Choi M Y, Kim J H, Cho J H and Lee W 2008 *Japanese Journal of Applied Physics* **47** 4705
[21] Kim H 2000 *Application of Non-thermal Plasma in Environmental Protection* Ph.D. thesis PhD Thesis, Toyohashi University of Technology, Toyohashi
[22] Zhang Y R, Van Laer K, Neyts E C and Bogaerts A 2016 *Applied Catalysis B: Environmental* **185** 56–67
[23] Fridman A, Chirokov A and Gutsol A 2005 *Journal of Physics D: Applied Physics* **38** R1

[24] Birdsall C K 1991 *Plasma Science, IEEE Transactions on* **19** 65–85
[25] Nieter C and Cary J R 2004 *Journal of Computational Physics* **196** 448–473
[26] Wild R, Benduhn J and Stollenwerk L 2014 *Journal of Physics D: Applied Physics* **47** 435204
[27] Lazarou C, Belmonte T, Chiper A and Georghiou G 2016 *Plasma Sources Science and Technology* **25** 055023
[28] Lieberman M A and Lichtenberg A J 2005 *Principles of plasma discharges and materials processing* (John Wiley & Sons)
[29] Furman M and Pivi M 2002 *Physical Review Special Topics-Accelerators and Beams* **5** 124404
[30] Phelps A and Petrovic Z L 1999 *Plasma Sources Science and Technology* **8** R21
[31] Pancheshnyi S, Biagi S, Bordage M, Hagelaar G, Morgan W, Phelps A and Pitchford L 2012 *Chemical Physics* **398** 148–153
[32] retrieved on June 11 2015 *Biagi-v8.9 database* URL `www.lxcat.net`
[33] Babaeva N Y and Kushner M J 2009 *Plasma Sources Science and Technology* **18** 035009
[34] Lofthus A and Krupenie P H 1977 *Journal of Physical and Chemical Reference Data* **6** 113–307
[35] Guerra V, Sá P and Loureiro J 2004 *The European Physical Journal Applied Physics* **28** 125–152
[36] Xiong Z, Robert E, Sarron V, Pouvesle J M and Kushner M J 2012 *Journal of Physics D: Applied Physics* **45** 275201
[37] Innocenti M E, Lapenta G, Markidis S, Beck A and Vapirev A 2013 *Journal of Computational Physics* **238** 115–140
[38] Avaria G, Grisham M, Li J, Tomasel F, Shlyaptsev V, Busquet M, Woolston M and Rocca J 2015 *Physical review letters* **114** 095001
[39] Kim H H, Teramoto Y, Sano T, Negishi N and Ogata A 2015 *Applied Catalysis B: Environmental* **166** 9–17
[40] Bhoj A N and Kushner M J 2008 *Plasma Sources Science and Technology* **17** 035024
[41] Kim H H and Ogata A 2011 *The European Physical Journal Applied Physics* **55** 13806
[42] Zhang Y R, Neyts E C and Bogaerts A 2016 *The Journal of Physical Chemistry C* **120** 25923–25934
[43] Kogelschatz U 2010 Collective phenomena in volume and surface barrier discharges *Journal of Physics: Conference Series* vol 257 (IOP Publishing) p 012015
[44] Jiang W, Peng Y, Zhang Y and Lapenta G 2016 *Nuclear Fusion* **56** 126017

8. Tables and table captions

Reaction	Threshold (eV)	Reference
Electron-impact ionization		[32]
$e + O_2 \rightarrow 2e + O_2^+$	12.06	
$e + N_2 \rightarrow 2e + N^{2+}$	15.58	
Attachment		[32]
$e + O_2 \rightarrow O_2^-$		
Electron-impact excitation		[32]
$e + O_2 \rightarrow e + O_2$		
$e + O_2 \rightarrow e + O_2^*$	0.98	
$e + O_2 \rightarrow e + O_2^*$	1.63	
$e + O_2 \rightarrow e + O_2^*$	6.0	
$e + O_2 \rightarrow e + O_2^*$	8.4	
$e + O_2 \rightarrow e + O_2^*$	10.0	
$e + N_2 \rightarrow e + N_2$		
$e + N_2 \rightarrow e + N_2^*$	6.169	
$e + N_2 \rightarrow e + N_2^*$	7.353	
$e + N_2 \rightarrow e + N_2^*$	7.362	
$e + N_2 \rightarrow e + N_2^*$	8.165	
$e + N_2 \rightarrow e + N_2^*$	8.399	
$e + N_2 \rightarrow e + N_2^*$	8.549	
$e + N_2 \rightarrow e + N_2^*$	8.89	
$e + N_2 \rightarrow e + N_2^*$	9.7537	
$e + N_2 \rightarrow e + N_2^*$	11.032	
$e + N_2 \rightarrow e + N_2^*$	12.771	
$e + N_2 \rightarrow e + N_2^*$	13.37	
$e + N_2 \rightarrow e + N_2^*$	13.382	
$e + N_2 \rightarrow e + N_2^*$	14.0	
Radiation	Rate coefficient	[34,35]
$N_2^* \rightarrow N_2 + h\upsilon$	$2\times10^5\ s^{-1}$	
Photo-ionization	Cross-section	[33]
$h\upsilon + O_2 \rightarrow e + O_2+$	$10^{-22}\ m^2$	

Table 1. Elastic, excitation, ionization and attachment reactions of electrons with N_2 and O_2, with the cross sections adopted from the LXCat database[32], as well as radiation and photo-ionization reactions applied in the photo-ionization model, with the rate coefficient for the radiation adopted from references[34, 35], and the cross section for photo-ionization taken from[33].

9. Figures and figure captions

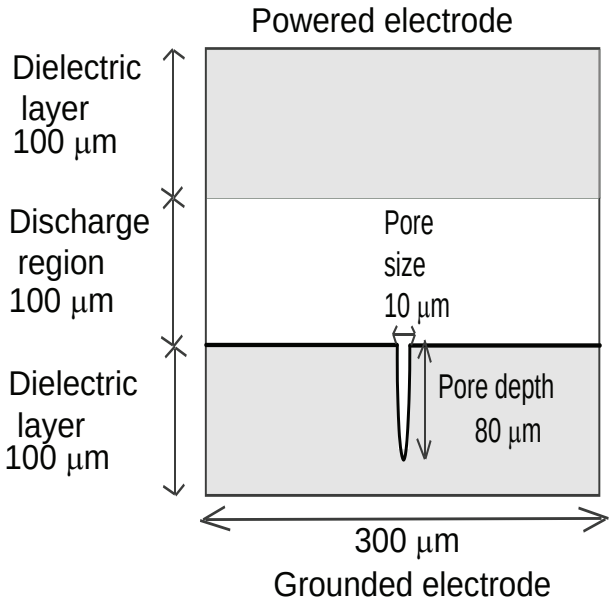

Figure 1. Geometry used in model 1. The 100 μm discharge gap is bounded by 100 μm thick dielectric plates at both the top and the bottom, which are both covered by metal electrodes. The upper electrode ($y = 300$ μm) is powered, while the bottom electrode ($y = 0$) is grounded. The bottom dielectric has a pore of 10 μm diameter, and the depth is 8 times the diameter.

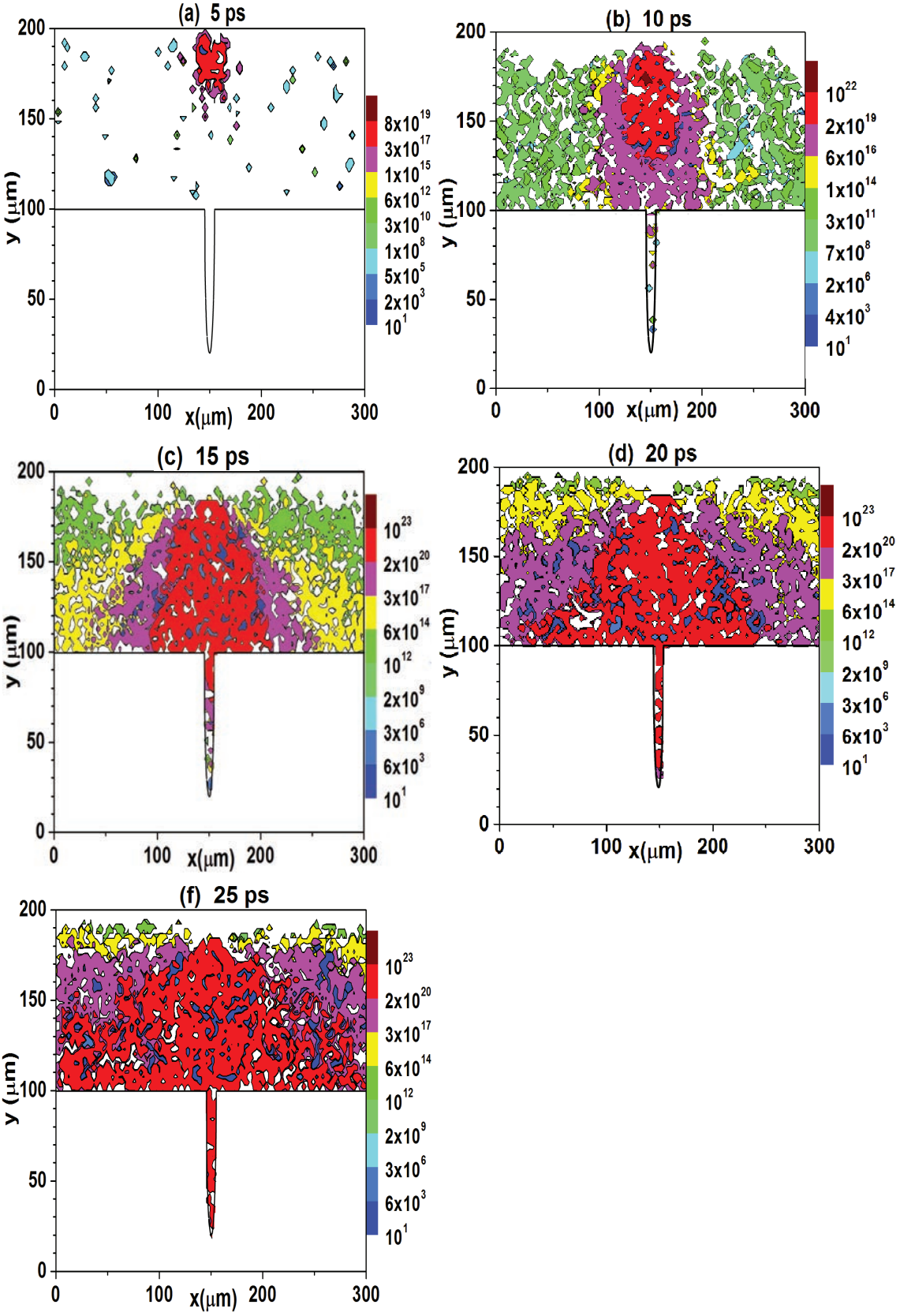

Figure 2. Electron density (m^{-3}) at 5, 10,15, 20 and 25 ps, in a DBD with $\epsilon_r = 4$ for both the top and bottom dielectric plate shown in Fig. 1. The size of the catalyst pore is 10 μm. The same lower color scale is used to allow comparison, while the upper color scale represents the maximum, respectively.

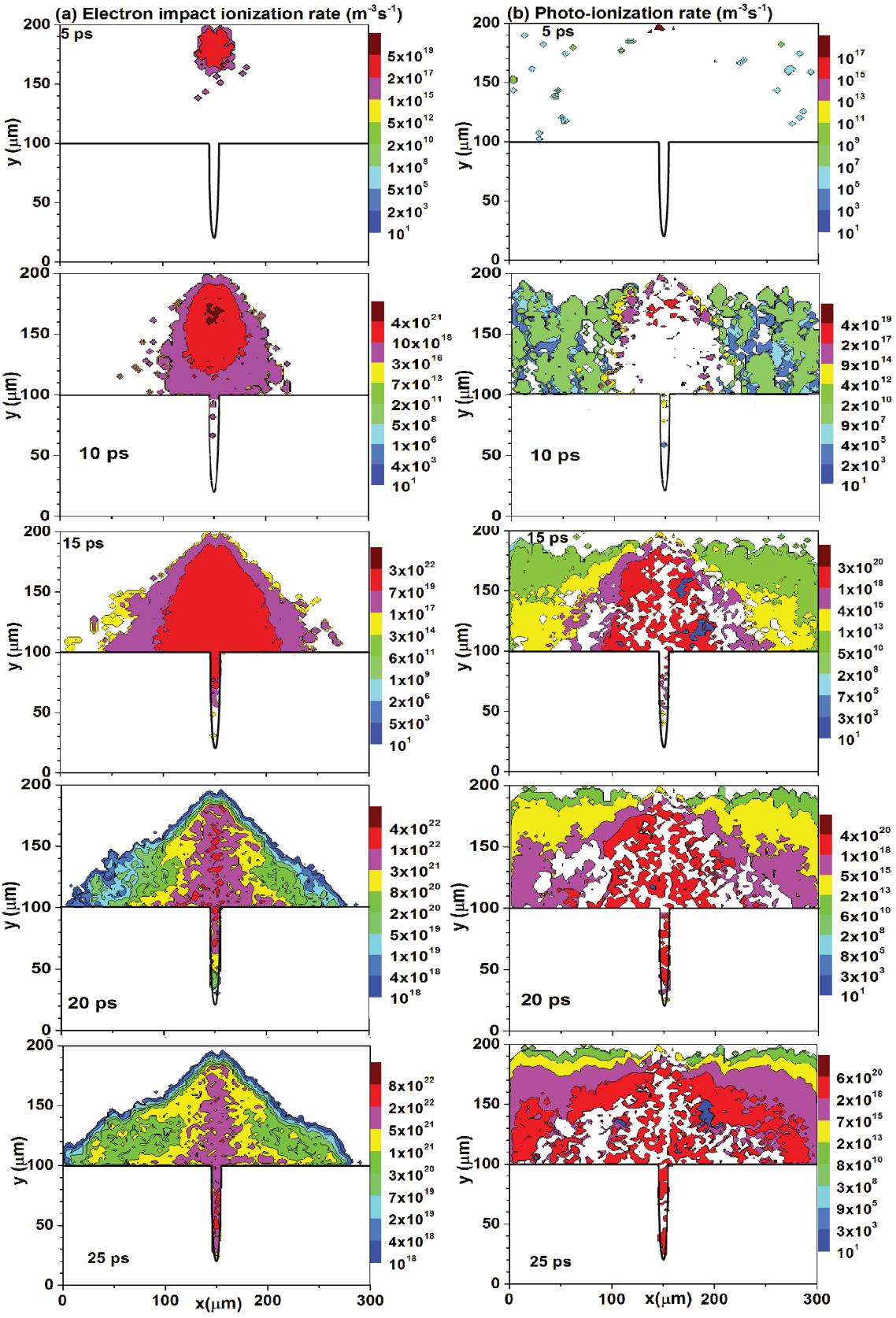

Figure 3. (a) Electron impact ionization rate ($m^{-3}s^{-1}$) and (b) photo-ionization rate ($m^{-3}s^{-1}$) for the same conditions as in Fig. 2. The same lower color scale is used at 5, 10 and 15 ps to allow comparison between the two ionization rates, while the upper color scale represents the maximum, respectively. The electron impact ionization rate at 20 and 25 ps uses as lower color scale a value of 10^{18} in order to clearly show the maximum values occurred in the pore.

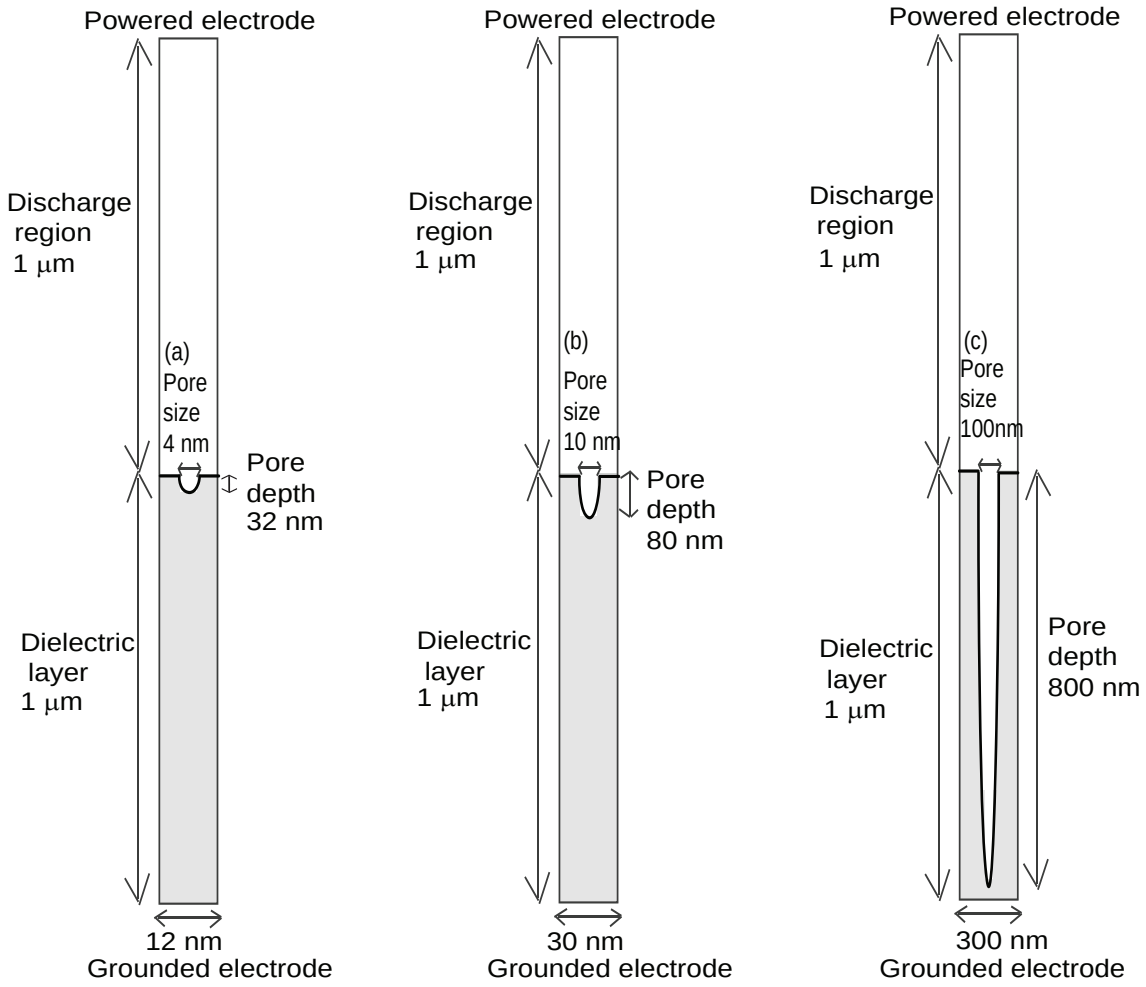

Figure 4. Geometry assumed in model 2. Note that the length scales in x and y dimensions are different, since it is really not possible to plot the same scales in x and y directions, which applies to all following figures. The distance between powered and grounded electrode is 2 μm. The grounded electrode is covered by a dielectric of 1μm thickness, resulting in a discharge gap of 1 μm. Illustrated here are pores with 4 nm (a), 10 nm (b) and 100 nm (c) in diameters and 32 nm (a), 80 nm (b) and 800 nm (c) of depths. All pores investigated in this work have a depth 8 times larger than the diameter. In the following, when mentioning the pore size, it refers to the pore diameter.

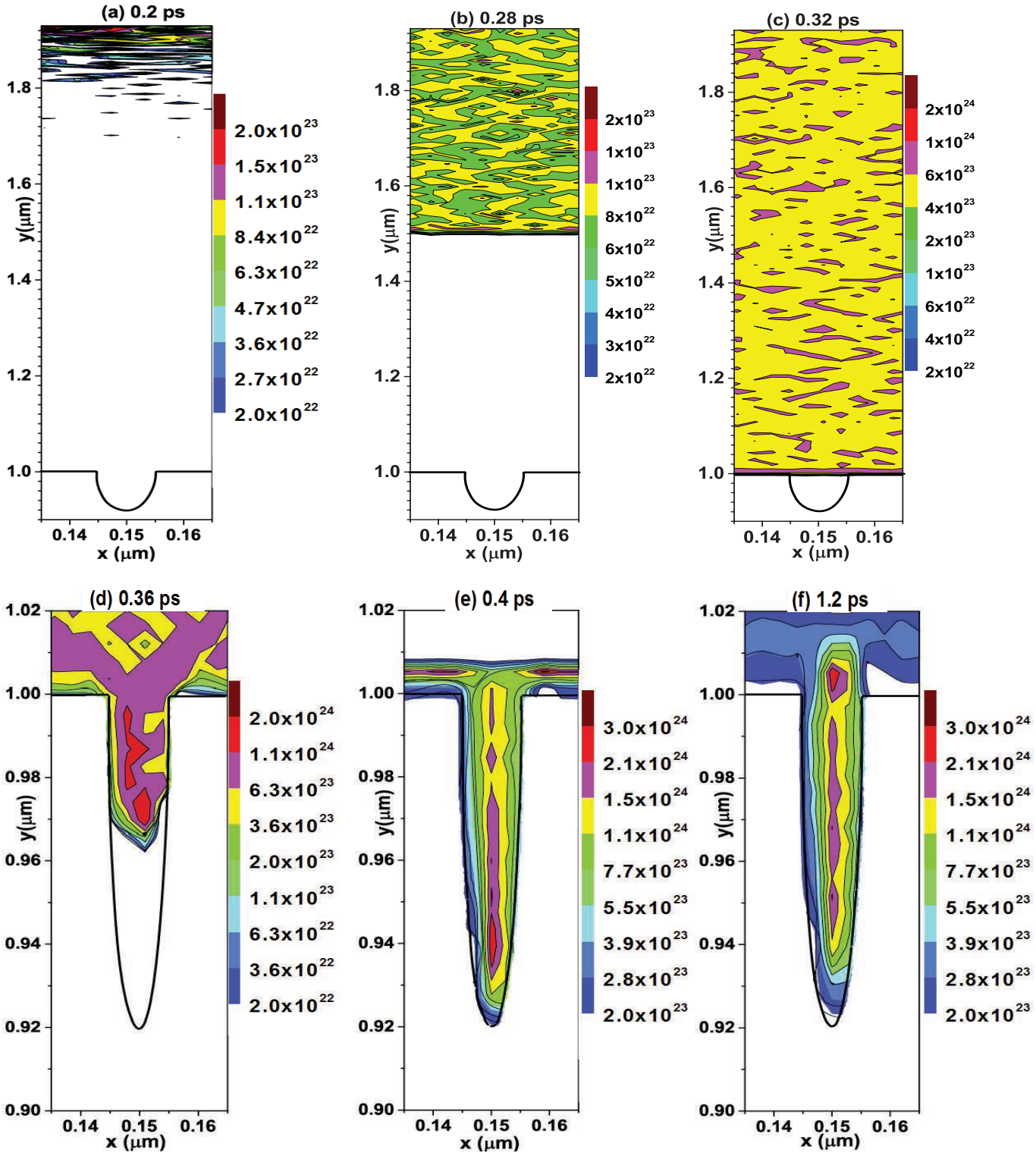

Figure 5. Electron density (m^{-3}) at 0.2, 0.28, 0.32, 0.36, 0.4 and 1.2 ps. The size of the catalyst pore is 10 nm. Note that the dimensions are different for (a-c), to visualize that the streamer does not yet reach the pore at this time.

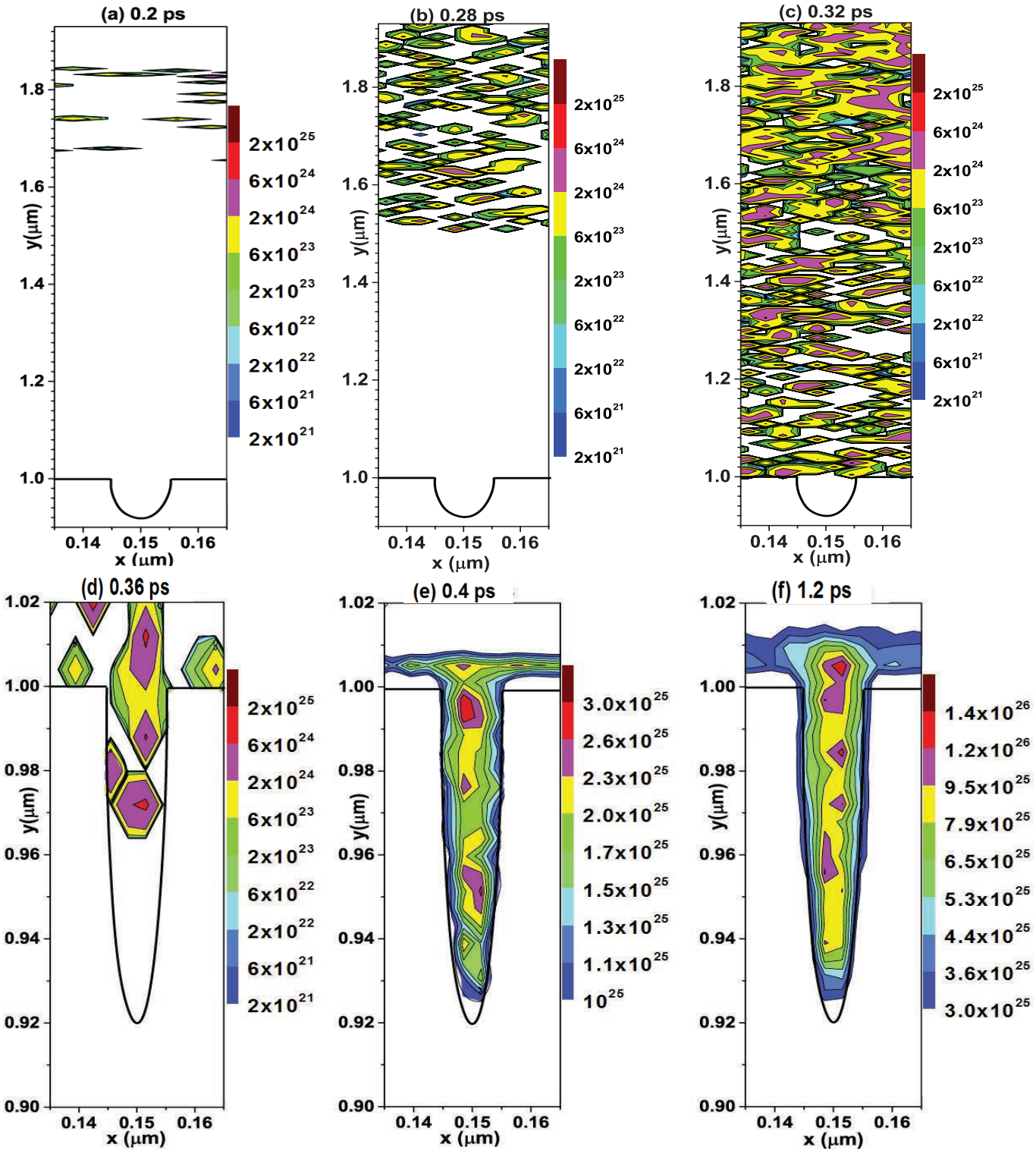

Figure 6. Electron impact ionization rate ($m^{-3}s^{-1}$) at the same conditions as in Fig. 5. Note that the dimensions are different for (a-c), to visualize that the streamer does not yet reach the pore at this time.

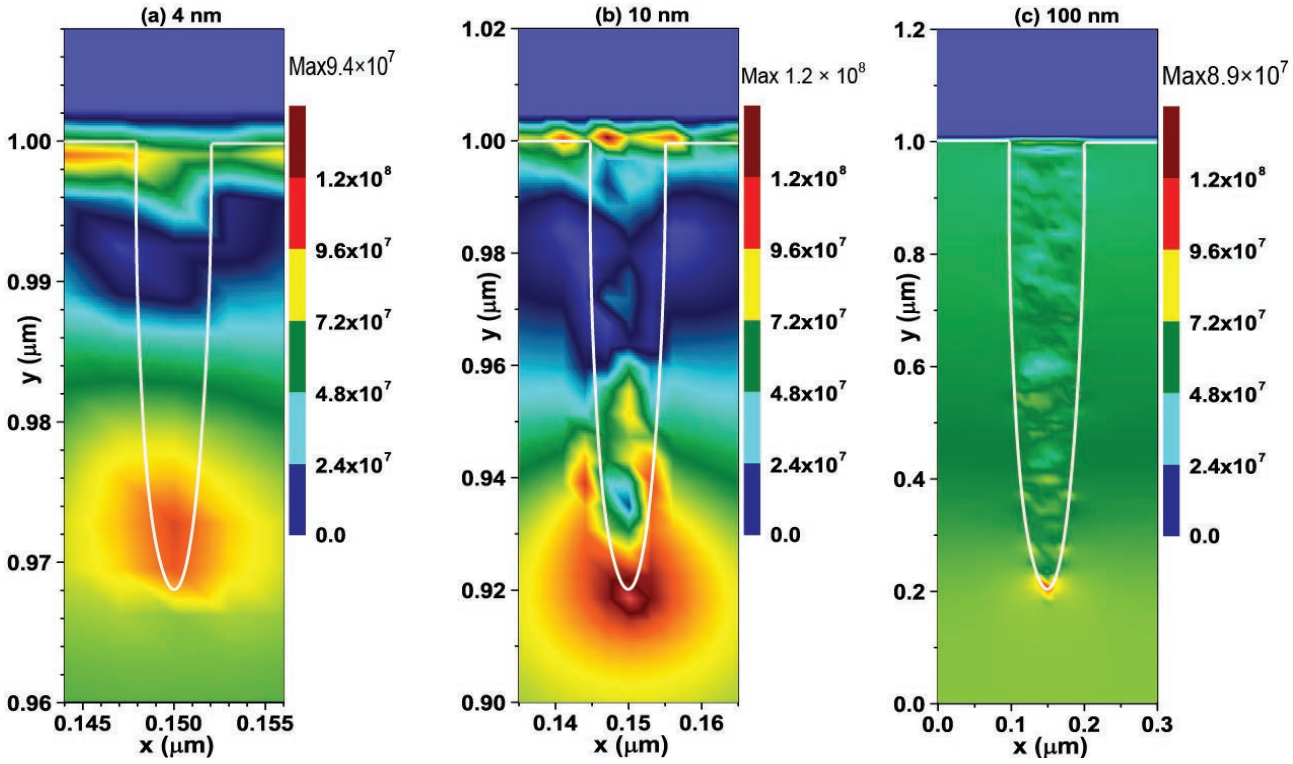

Figure 7. Distributions of the electric field (V/m) inside the pore and the dielectric material, for different pore sizes, at 1.2 ps. The same color scale is used for all three pores, to allow comparison, but the values above the color scale indicate the maximum value in each case.

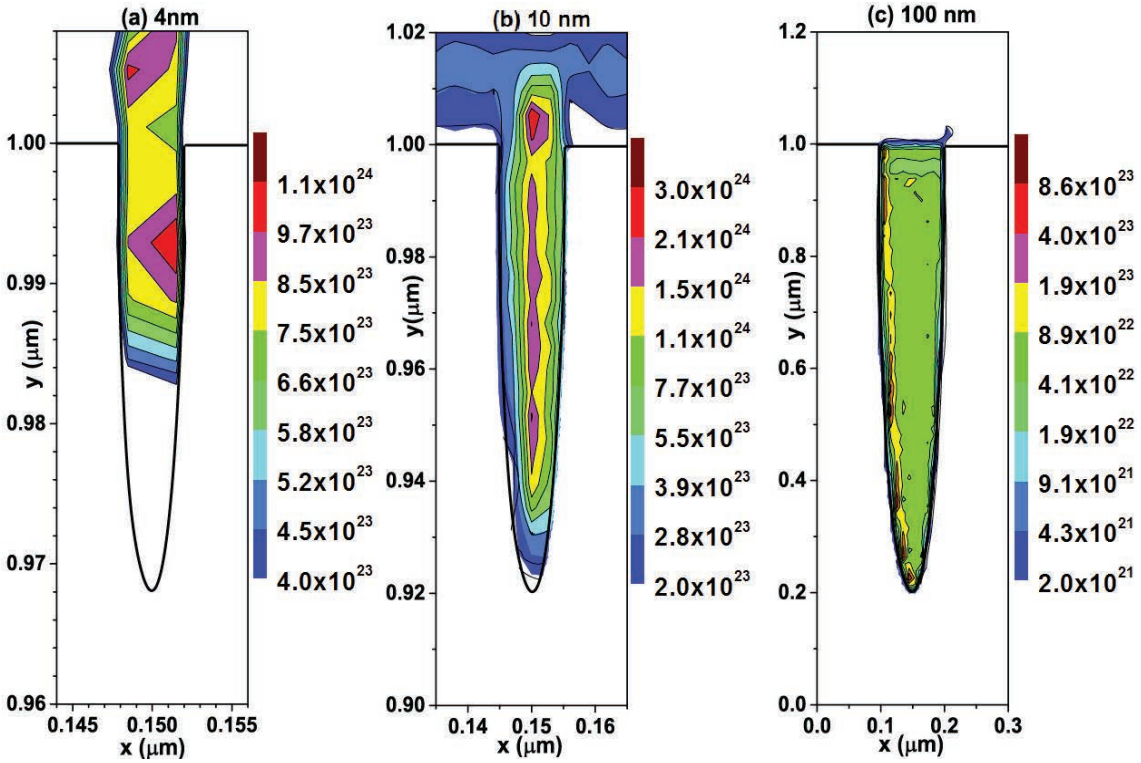

Figure 8. Distributions of the electron density (m^{-3}) in different pores, at 1.2 ps.

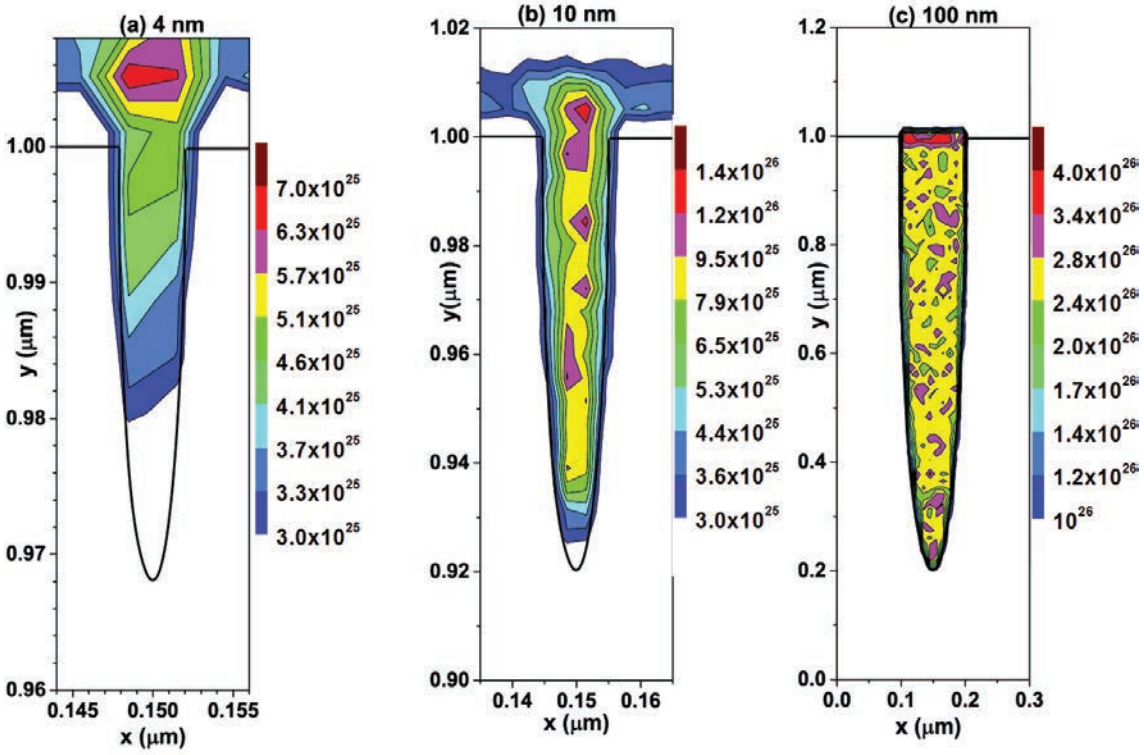

Figure 9. Distributions of the electron impact ionization rate ($m^{-3}s^{-1}$) in different pores, at 1.2 ps.

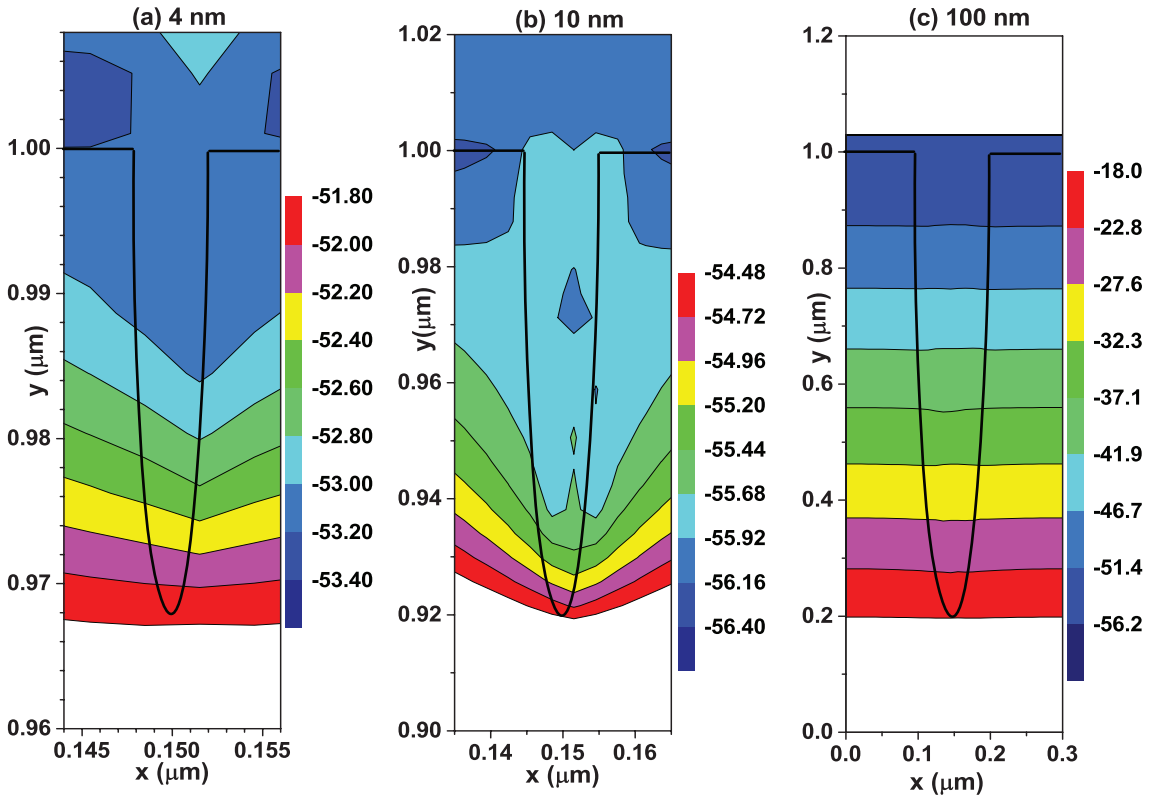

Figure 10. Electric potential (V) distribution for different pores, at 1.2 ps.

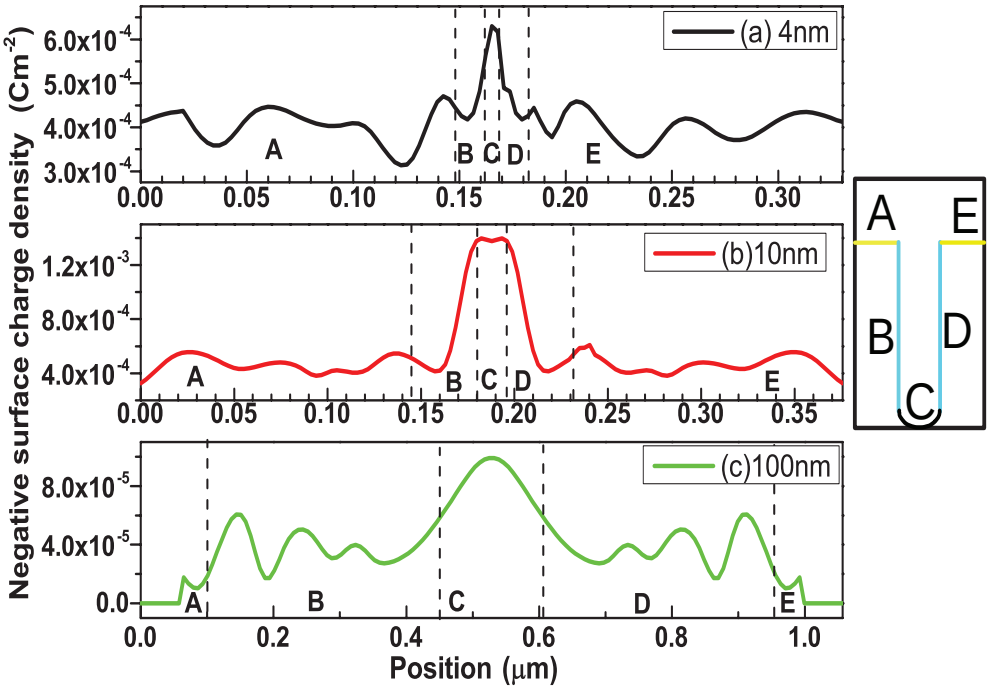

Figure 11. Negative surface charge density (Cm^{-2}), at the lower dielectric surface outside of the pore (A and E), the pore sidewalls (B and D), and the pore bottom (C), for different pore sizes, at 1.2 ps.

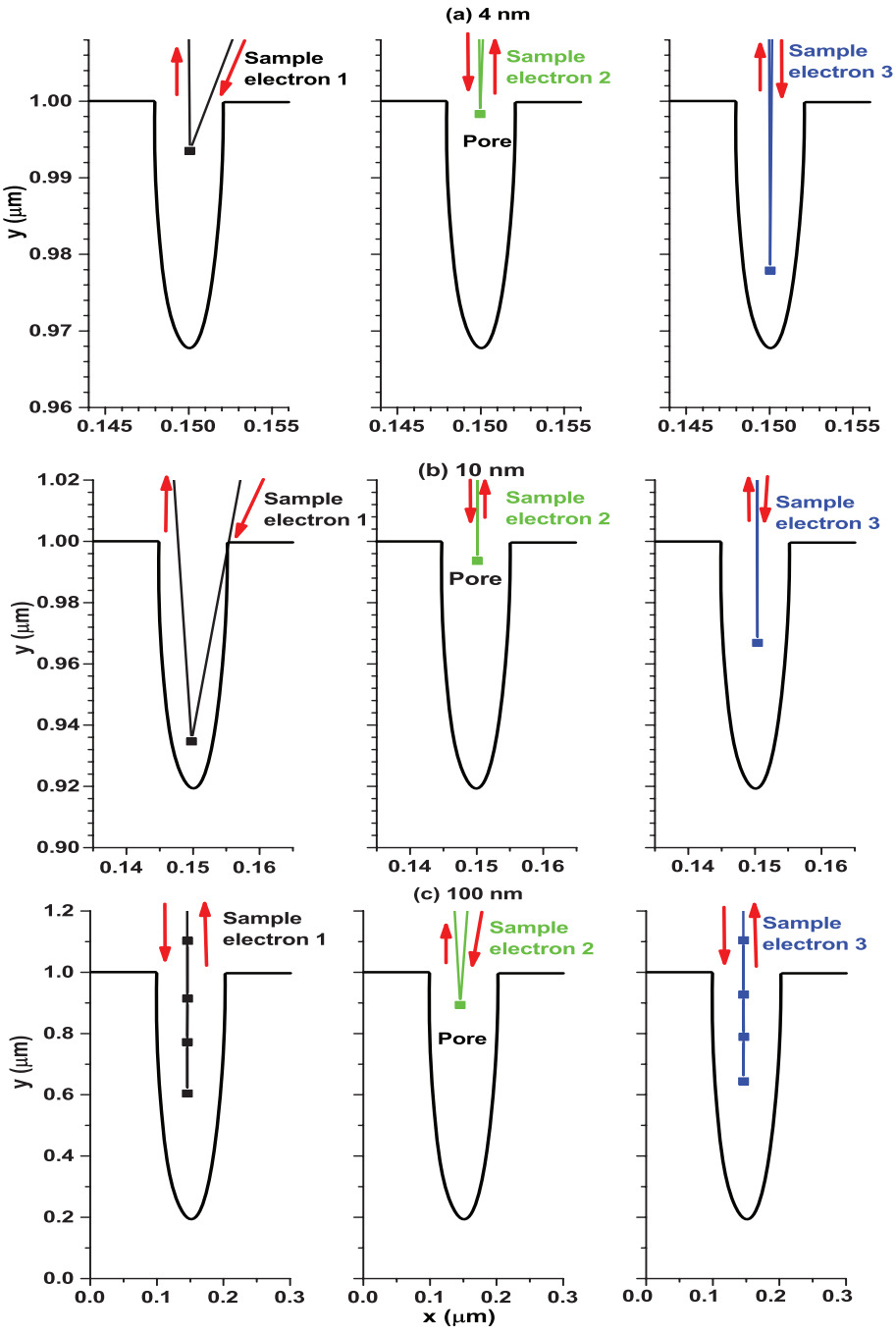

Figure 12. Electron trajectory of 3 different sample electrons for the 4, 10 and 100 nm pores.

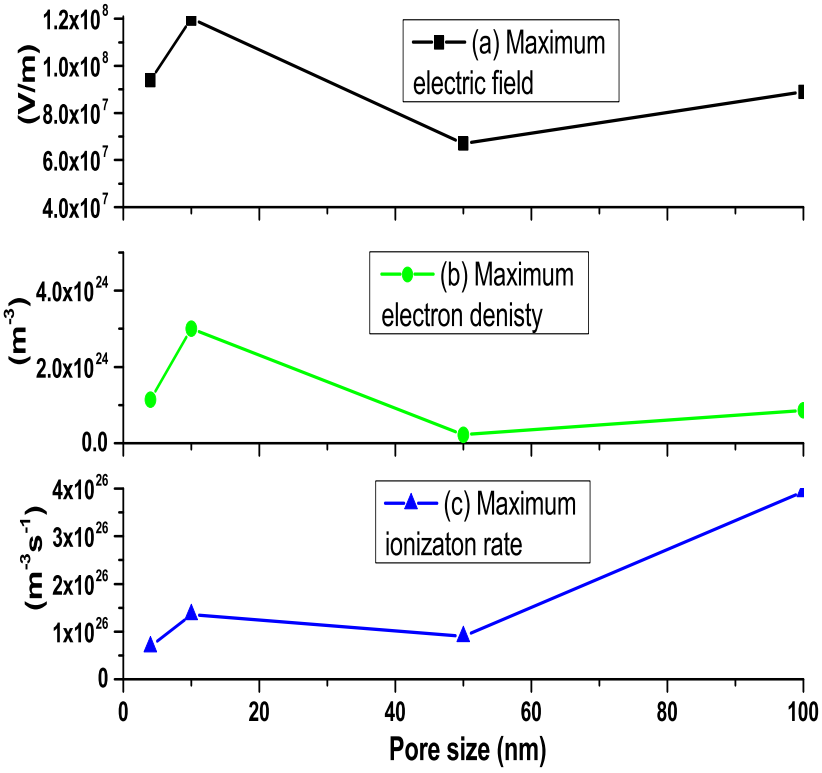

Figure 13. Maximum electric field (V/m), electron density (m^{-3}) and electron impact ionization rate ($m^{-3}s^{-1}$) as a function of pore size, at 1.2 ps.